

Surface tension effects on the behavior of a cavity growing, collapsing, and rebounding near a rigid wall

Zhen-yu Zhang* and Hui-sheng Zhang†

Department of Mechanics and Engineering Science, Fudan University, Shanghai 200433, People's Republic of China

(Received 1 April 2004; revised manuscript received 24 June 2004; published 19 November 2004)

Surface tension effects on the behavior of a pure vapor cavity or a cavity containing some noncondensable contents, which is growing, collapsing, and rebounding axisymmetrically near a rigid wall, are investigated numerically by the boundary integral method for different values of dimensionless stand-off parameter γ , buoyancy parameter δ , and surface tension parameter β . It is found that at the late stage of the collapse, if the resultant action of the Bjerknes force and the buoyancy force is not small, surface tension will not have significant effects on bubble behavior except that the bubble collapse time is shortened and the liquid jet becomes wider. If the resultant action of the two force is small enough, surface tension will have significant and in some cases substantial effects on bubble behavior, such as changing the direction of the liquid jet, making a new liquid jet appear, in some cases preventing the bubble from rebound before jet impact, and in other cases causing the bubble to rebound or even recollapse before jet impact. The mechanism of surface tension effects on the collapsing behavior of a cavity has been analyzed. The mechanisms of some complicated phenomena induced by surface tension effects are illustrated by analysis of the computed velocity fields and pressure contours of the liquid flow outside the bubble at different stages of the bubble evolution.

DOI: 10.1103/PhysRevE.70.056310

PACS number(s): 47.55.Bx, 47.55.Dz, 47.15.Hg

I. INTRODUCTION

The collapse of a cavity near a rigid wall has been studied extensively in connection with the pitting and erosion of hydraulic machinery and recently with laser surgery. Because of the complexity of physics involved in this process, additional phenomena are constantly found when the ambient flow conditions are changed, or the experimental and numerical simulation techniques are improved. For example, early it was thought from the work of Rayleigh for a spherical vapor bubble [1] that the pitting and erosion were caused by high pressure close to the cavity surface during its collapse. By use of spark- or laser-generated cavities and high-speed photographs it has been observed in experiments that during the later stage of collapse of a cavity near a rigid wall a high-speed jet forms, develops, impacts, and penetrates the opposite side of the cavity surface, and, in the absence of significant opposing buoyancy forces, is directed normally to the wall; finally, a toroidal bubble forms [2–7]. Then attention concerning the mechanism of damage was focused on the jet impact. When γ , the ratio of the distance between the inception point of a cavity and the wall to the maximum cavity radius, is greater than 1.2, the peak pressures recorded on the wall for a cavity of a given maximum radius increase monotonically as the location of the cavity inception is moved closer to the wall. The peak pressures are identified as due to the shock waves radiated as the cavity rebounds from minimum volume. For $0.6 < \gamma < 1.2$, however, the peak pressures decrease as γ decreases. When $0.8 < \gamma < 1.2$ it is observed that the radial flow outward along the wall induced by jet impact on a thin liquid layer separating the cavity from

the wall meets the inflow due to the contracting cavity, and generates a splash which impacts violently on the surface of the cavity [8–11]. The combination of splash impact and the emission of shock waves, together with the rebounding, results in a flow around the toroidal cavity and produces a distinctive double pressure peak, the first of which is associated with short-lived shock pressures and the second of which corresponds to the high pressures of longer duration produced by the subsequent flow around the toroidal cavity and the start of rebound of the cavity. Hydrodynamic pressures generated following splash impact are found to be much higher than those of jet impact and might be responsible for the annular damage of the wall. By using high-speed cinematography with 10^8 frames per second and long-distance microscopy, evidence has been provided experimentally that the counterjet is not part of the bubble but is composed of many tiny cavities which are generated by a tension wave following one of the moving intersection points (above the bubble) of the inward propagation part of the jet torus shock wave [12]. The counterjet can emerge only when $1 < \gamma < 3$. When $0.6 < \gamma < 1$, splash occurs. When $\gamma < 0.6$ no splash can be observed. The maximum volume compression reaches a minimum at $\gamma = 1.0$ and increases dramatically when $\gamma \rightarrow 0$ or $\gamma \rightarrow \infty$.

It is difficult, however, to provide experimentally the detailed information of velocity and pressure fields of flow induced by a cavity growing, collapsing, and rebounding near a rigid wall. Because the available theoretical analysis is limited to asymptotic studies in which deformation of the bubble is confined to a small perturbation to the spherical shape [4], numerical simulation has become an important tool for investigation of the detailed physics of this phenomenon. Using a vortex-in-cell type finite difference approach Ref. [13] conducted, in the absence of the buoyancy force, the first fully numerical study on the axisymmetric collapse of an

*Email address: zhangzhenyu@cableplus.com.cn

†Corresponding author; email address: hszhang@fudan.edu.cn

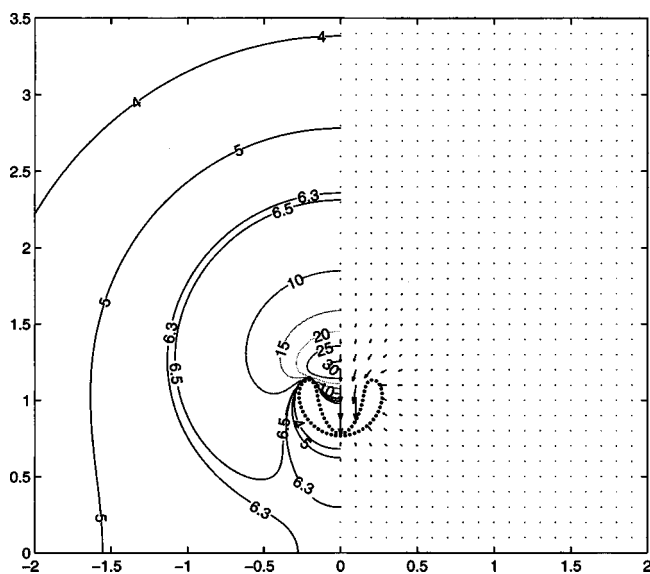


FIG. 1. (Color online) Bubble profile, velocity field, and pressure contours just before jet impact for $\gamma=1.5$, $\alpha=0$, $\beta=0$, $\delta=0$, and $R_0=0.1$.

initially spherical cavity near a rigid wall. Recently Ref. [14] provided a numerical investigation of the problem by use of a second order coupled level set and the volume-of-fluid (VOF) method. Because of the high Reynolds number of the flow induced by a transient cavity and the self-adaptive deformation of the bubble, which makes the occurrence of flow separation not easy [15], the boundary integral method based on potential flow theory has achieved great successes in the numerical simulation of hydraulic cavitation phenomena. By this method an axisymmetric cavity near a rigid wall has been studied numerically by lots of work. Reference [16] simulated the growth and collapse in the presence of the buoyancy force and an incident stagnation-point flow which is a model of flow near a reattachment point of the boundary layer, a region where the most severe cavitation damage occurs, and showed the importance of the growing phase to the behavior of the collapse phase. Reference [17] investigated the growth, collapse, and rebound in the presence of buoyancy force and noncondensable contents in the cavity. By introducing, after jet impact, a cut across which the velocity

potential is discontinuous, the value of the discontinuity being equal to the circulation in the flow, the boundary integral method has been developed by Ref. [18] to allow a continuous simulation from growth to collapse and the jet impact and penetrating. Reference [19] extended the work of Ref. [18] to incorporate a vortex sheet. Using the method of Ref. [18], Refs. [8,9] and [11] modeled the splash phenomena induced by the bubble collapse and jet impact. Also by the boundary integral method Refs. [20–22] investigated three-dimensional jet impact and toroidal bubbles.

None of the works mentioned above considered and analyzed surface tension effects. However, in some cases, for example, when the cavity is small, or as pointed out by Ref. [16], when the cavity collapses under a small difference between the saturated vapor pressure p_c inside the cavity and the ambient pressure p_∞ outside it (in practical hydraulic machinery flows a cavity can occur and grow at a place where $p_\infty < p_c$ and then begin to collapse at a place downstream where $p_\infty > p_c$ but the pressure difference $\Delta p = p_\infty - p_c$ is not large), surface tension effects could be important. In the numerical simulation of a Crum bubble, Ref. [23] incorporated a surface tension term in the governing equations. The purpose of this paper is, by the boundary integral method, to investigate numerically the effects of surface tension on the behavior of a cavity growing, collapsing, and rebounding axisymmetrically near a rigid wall.

II. GOVERNING EQUATIONS AND NUMERICAL METHODS

Suppose a liquid of density ρ is filled in a domain D , where D is above an infinite and rigid plane wall $z=0$ and outside a cavity with boundary S and saturated vapor pressure p_c . The Cartesian coordinates are chosen such that the gravity is along the z direction. It is assumed that p_c is a constant and initially the liquid is stationary and the cavity is in a spherical shape with its center at $(x, y, z) = (0, 0, z_0)$. So the flow in D is axisymmetric. The assumption that the liquid is incompressible and inviscid leads to the irrotationality of the flow. Therefore the flow velocity $\mathbf{u} = \nabla \phi$ and the potential ϕ satisfies the Laplace equation. Thus ϕ satisfies the equation

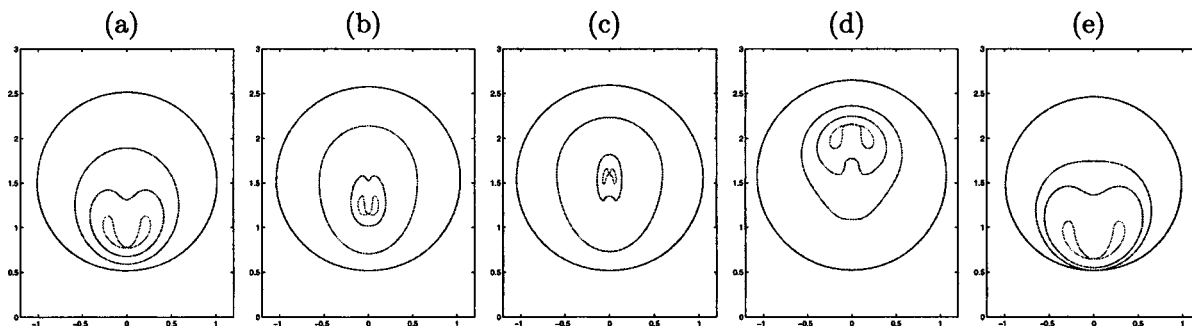


FIG. 2. (Color online) Bubble profiles during collapse phase for $\gamma=1.5$, $\alpha=0$, $R_0=0.1$, and $\beta=0$. From leftmost to rightmost: $\delta=0$, 0.05, 0.063, 0.1, and -0.05 . In the subfigures, from outermost to innermost, the nondimensional times are (a) 1.048, 1.921, 2.024, 2.075; (b) 1.121, 2.070, 2.209, 2.220; (c) 1.145, 2.090, 2.259, 2.264; (d) 1.215, 2.274, 2.368, 2.407; (e) 0.989, 1.767, 1.848, 1.953.

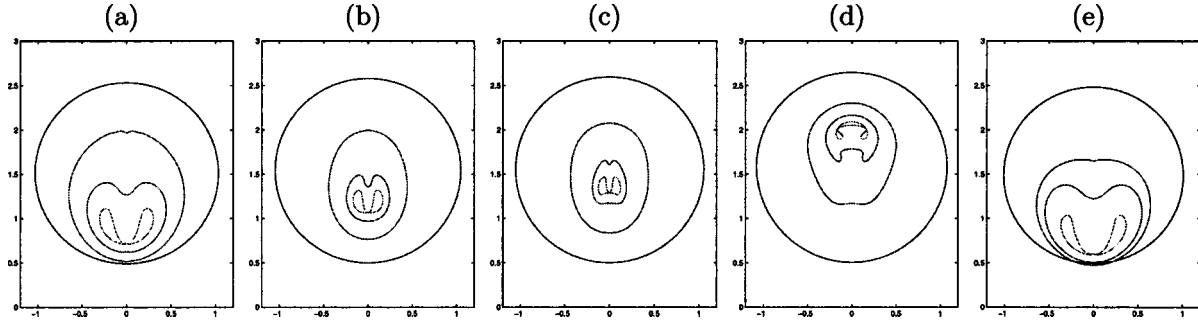


FIG. 3. (Color online) Bubble profiles during collapse phase for $\gamma=1.5$, $\alpha=0$, $R_0=0.1$, and $\beta=0.05$. From leftmost to rightmost: $\delta=0$, 0.05, 0.063, 0.1, and -0.05 . In the subfigures, from outermost to innermost, the nondimensional times are (a) 1.026, 1.828, 1.964, 2.017; (b) 1.079, 2.046, 2.115, 2.127; (c) 1.095, 2.085, 2.158, 2.165; (d) 1.156, 2.196, 2.273, 2.294; (e) 0.971, 1.748, 1.823, 1.910.

$$\int \int_S \left[G(\mathbf{x}, \mathbf{y}) \frac{\partial \phi(\mathbf{y})}{\partial \mathbf{n}} - [\phi(\mathbf{y}) - \phi(\mathbf{x})] \frac{\partial G(\mathbf{x}, \mathbf{y})}{\partial \mathbf{n}} \right] dS(\mathbf{y}) = 4\pi\phi(\mathbf{x}), \quad \mathbf{x} \in D \cup S, \quad (1)$$

where \mathbf{n} is the inward unit normal on S and $G(\mathbf{x}, \mathbf{y})$ is the Green's function defined by

$$G(\mathbf{x}, \mathbf{y}) = \frac{1}{|\mathbf{x} - \mathbf{y}|} + \frac{1}{|\tilde{\mathbf{x}} - \mathbf{y}|}.$$

Here $\tilde{\mathbf{x}}$ is the image of the position vector \mathbf{x} with respect to the plane mirror $z=0$. The Bernoulli equation is

$$\frac{\partial \phi}{\partial t} + \frac{1}{2}u^2 + \frac{p}{\rho} + g(z - z_0) = \frac{p_\infty}{\rho}, \quad \mathbf{x} \in D \cup S, \quad (2)$$

where $u = |\mathbf{u}|$, p_∞ is the ambient pressure at $z=z_0$, and g is the gravity acceleration with positive or negative value corresponding to the gravity being in the direction to the wall or away from the wall, respectively. The pressure p_b inside the cavity is assumed to be uniform and is expressed by

$$p_b = p_b(t) = p_c + p_0 \left(\frac{V_0}{V} \right)^\kappa, \quad (3)$$

where $V = V(t)$ is the bubble volume, p_0 is the pressure of the noncondensable contents inside the cavity when $V = V_0$, and κ is the ratio of specific heats (in this paper κ is taken to be 1.4). The liquid pressure p on S satisfies

$$p = p_b + \sigma \nabla \cdot \mathbf{n} \quad (4)$$

where σ is the surface tension on S . Substituting Eqs. (3) and (4) into Eq. (2) on S yields

$$\begin{aligned} \frac{d\phi}{dt} &= \frac{\partial \phi}{\partial t} + \mathbf{u} \cdot \nabla \phi \\ &= \frac{\Delta p}{\rho} + \frac{1}{2}u^2 - \frac{p_0}{\rho} \left(\frac{V_0}{V} \right)^\kappa - \frac{\sigma}{\rho} \nabla \cdot \mathbf{n} - g(z - z_0), \quad \mathbf{x} \in S \end{aligned} \quad (5)$$

where $\Delta p = p_\infty - p_c$. Let R_m be the maximum equivalence radius of the bubble. In this problem $\gamma = z_0/R_m$ is an important dimensionless parameter. By introducing the dimensionless quantities

$$\hat{\mathbf{x}} = \frac{\mathbf{x}}{R_m}, \quad \hat{t} = \frac{t\sqrt{\Delta p/\rho}}{R_m}, \quad \hat{\mathbf{u}} = \mathbf{u}\sqrt{\rho/\Delta p}, \quad \hat{\phi} = \frac{\phi\sqrt{\rho/\Delta p}}{R_m},$$

$$\hat{p} = \frac{p - p_c}{\Delta p}$$

and omitting the caret notation over all of the dimensionless quantities, the dimensionless form of Eq. (1) is kept

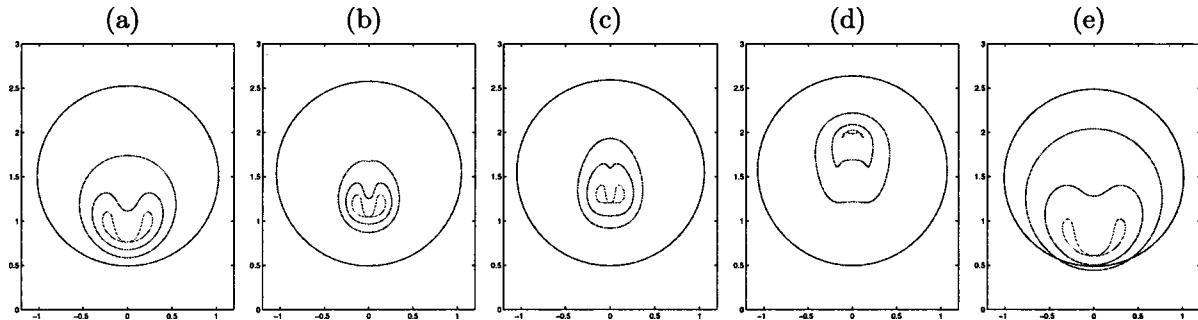


FIG. 4. (Color online) Bubble profiles during collapse phase for $\gamma=1.5$, $\alpha=0$, $R_0=0.1$, and $\beta=0.1$. From leftmost to rightmost: $\delta=0$, 0.05, 0.063, 0.1, and -0.05 . In the subfigures, from outermost to innermost, the nondimensional times are (a) 0.960, 1.806, 1.880, 1.914; (b) 1.020, 1.990, 2.013, 2.024; (c) 1.035, 2.012, 2.041, 2.056; (d) 1.090, 2.100, 2.153, 2.165; (e) 0.924, 1.553, 1.750, 1.840.

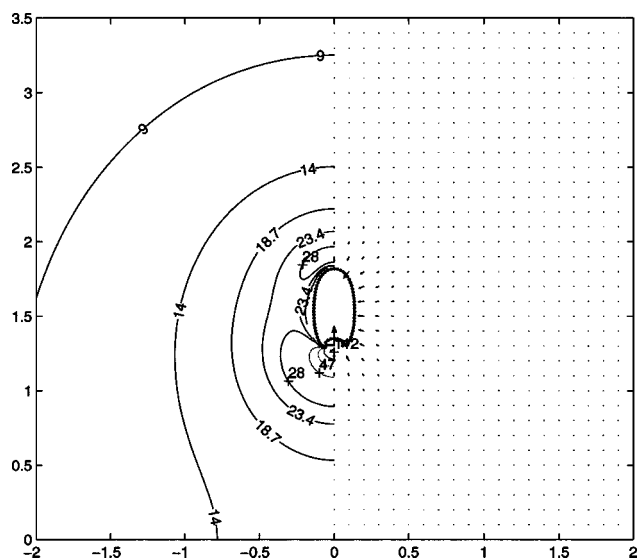


FIG. 5. (Color online) Velocity field and pressure contours at the time of jet inception for $\gamma=1.5$, $\alpha=0$, $\beta=0$, $\delta=0.063$, $R_0=0.1$, and $t=2.259$.

unchanged and the dimensionless forms of Eqs. (2) and (5) are, respectively,

$$\frac{\partial \phi}{\partial t} + \frac{1}{2}u^2 + p = 1, \quad \mathbf{x} \in D, \quad (6)$$

$$\frac{d\phi}{dt} = 1 + \frac{1}{2}u^2 - \alpha \left(\frac{V_0}{V} \right)^\kappa - \beta \nabla \cdot \mathbf{n} - \delta(z - z_0), \quad \mathbf{x} \in S, \quad (7)$$

where the dimensionless parameters α (compression ratio), β (the reciprocal of the Weber number), and δ (the relative importance of the buoyancy) are defined by

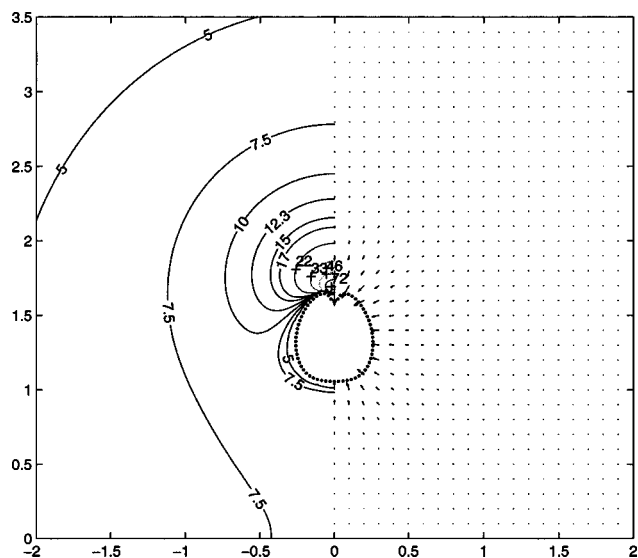


FIG. 6. (Color online) Velocity field and pressure contours at the time of jet inception for $\gamma=1.5$, $\alpha=0$, $\beta=0.1$, $\delta=0.063$, $R_0=0.1$, and $t=2.041$.

TABLE I. Collapse time t_c for $\gamma=1.5$, $\alpha=0$, $R_0=0.1$, and for different β and δ .

β	δ					
	0	0.05	0.063	0.1	-0.05	-0.1
0	1.026	1.099	1.119	1.192	0.965	0.919
0.05	0.991	1.048	1.070	1.137	0.940	0.892
0.1	0.954	1.003	1.021	1.074	0.912	0.875

$$\alpha = \frac{p_0}{\Delta p}, \quad \beta = \frac{\sigma}{R_m \Delta p}, \quad \delta = \frac{\rho g R_m}{\Delta p}.$$

For a spherical cavity with 1 mm diameter collapsing at pressure difference $\Delta p=1000$ Pa and at temperature 10°C , the value of β is about 0.15. Note that the parameter δ is just the square of that in Refs. [16–18].

The solution is as follows. Suppose at time t the bubble shape S and the potential on S are known. Thus at this time the tangential and normal velocities on S can be obtained by, respectively, calculating the tangential gradient of ϕ on S and solving the integral equation (1) for $\partial\phi/\partial n$ on S , and, if necessary, the potential ϕ and pressure p in the flow field D can be got in turn by calculating the integral on the left hand side of Eq. (1) and then using the Bernoulli equation (6). At time $t+\Delta t$ the bubble shape and potential on S can be obtained by time integrating the equation

$$\frac{d\mathbf{x}}{dt} = \mathbf{u}, \quad \mathbf{x} \in S, \quad (8)$$

and Eq. (7), respectively.

As the problem is axisymmetric the Green’s function can be integrated in the azimuthal direction, which reduces Eq. (1) into an integral equation on the semimeridian line of the bubble. The integrand of the reduced integral equation contains some complete elliptic integrals of the first and third kinds. Note that this kind of expression for Eq. (1) has the advantage that in the reduced integral equation the function corresponding to the second term in the integrand of Eq. (1) is smooth. The singularity contained in the complete elliptic integrals can be removed by subtracting a proper logarithm function. Thus the integrand of the reduced integral equation contains only smooth functions and products of a logarithm function and smooth functions. The initial value of the potential is taken as the Rayleigh spherical bubble solution in which the terms associated with the effects of image source, surface tension, and noncondensable contents are included,

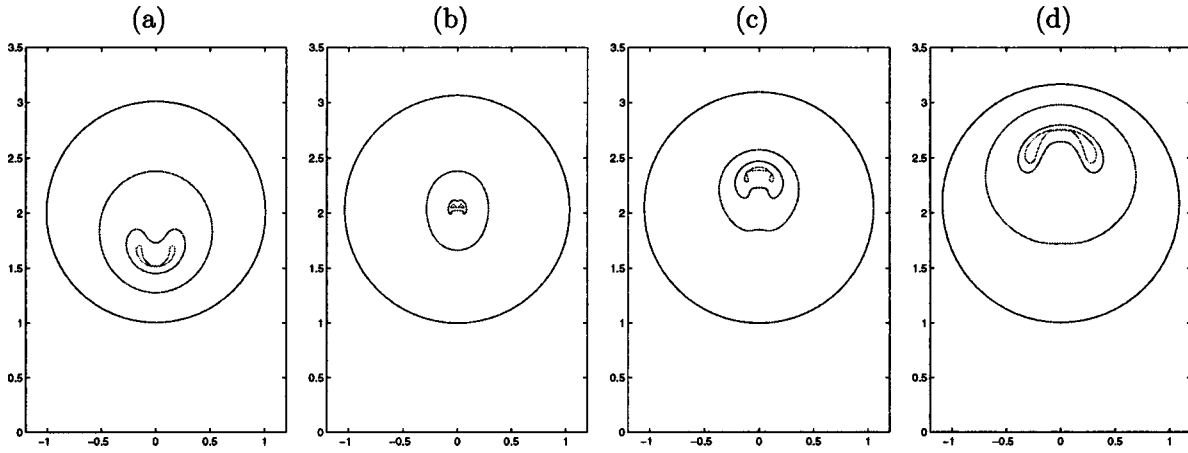


FIG. 7. (Color online) Bubble profiles during collapse phase for $\gamma=2$, $\alpha=0$, $R_0=0.1$, and $\beta=0$. From leftmost to rightmost: $\delta=0$, 0.04, 0.06, and 0.1. In the subfigures, from outermost to innermost, the nondimensional times are (a) 1.024, 1.908, 2.001, 2.015; (b) 1.096, 2.140, 2.165, 2.167; (c) 1.450, 2.214, 2.225, 2.257; (d) 1.248, 2.266, 2.416, 2.471.

$$\phi_0 = - \left(R_0 + \frac{R_0^2}{\sqrt{r^2 + (z+z_0)^2}} \right) \sqrt{\frac{2}{3} \left(\frac{1}{R_0^3} - 1 \right)} + 2\beta \left(\frac{1}{R_0^3} - \frac{1}{R_0} \right) + \frac{2\alpha}{3(1-\kappa)} [1 - R_0^{3(\kappa-1)}],$$

where r and z are the cylindrical coordinates and R_0 is the radius of the cavity at $t=0$.

To solve the problem numerically the semimeridian line is divided into N elements. In this paper we take $N=32$. The integral on the semimeridian line is then reduced to the sum of integrals on the N elements. Within any element ϕ , $\partial\phi/\partial n$ and the arc representing the bubble surface are approximated by linear interpolations based on their values at the end points of the element. On any element the integrals of smooth functions and those of functions containing a logarithmic singularity are integrated numerically by, respectively, four-point Gauss-Legendre quadrature and four-point Gaussian quadrature with the logarithm function as its weight [24]. In order to avoid numerical integration of a

smooth function with large gradient, on any element which does not contain any singularity point but is near a singularity point, the integral is pretreated by several times of integration by parts before it is integrated numerically. Spatial derivatives of unknown functions are approximated by second order centered finite differences. Thus the integral equation is reduced to a system of linear algebraic equations with the nodal point values of $\partial\phi/\partial n$ as the unknowns, and the partial differential equations (7) and (8) are reduced to a system of ordinary differential equations with the corresponding nodal point values as the unknown functions. In this paper the system of linear algebraic equations is solved by Gaussian elimination with partial pivot. The numerical method suffers the Courant-Friedrichs-Lewy (CFL) type in-

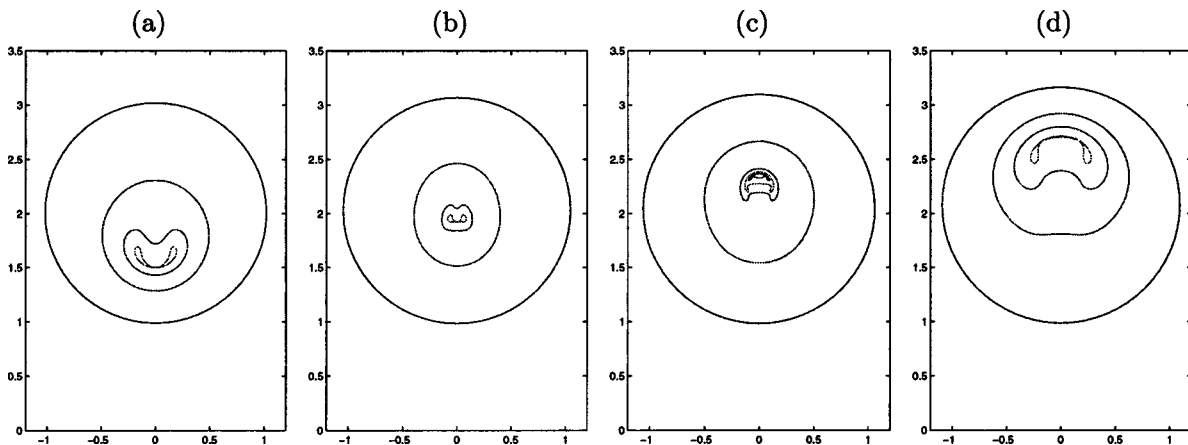


FIG. 8. (Color online) Bubble profiles during collapse phase for $\gamma=2$, $\alpha=0$, $R_0=0.1$, and $\beta=0.05$. From leftmost to rightmost: $\delta=0$, 0.04, 0.06, and 0.1. In the subfigures, from outermost to innermost, the nondimensional times are (a) 0.980, 1.858, 1.926, 1.942; (b) 1.050, 2.020, 2.070, 2.073; (c) 1.093, 2.058, 2.147, 2.151, 2.153; (d) 1.180, 2.195, 2.301, 2.342.

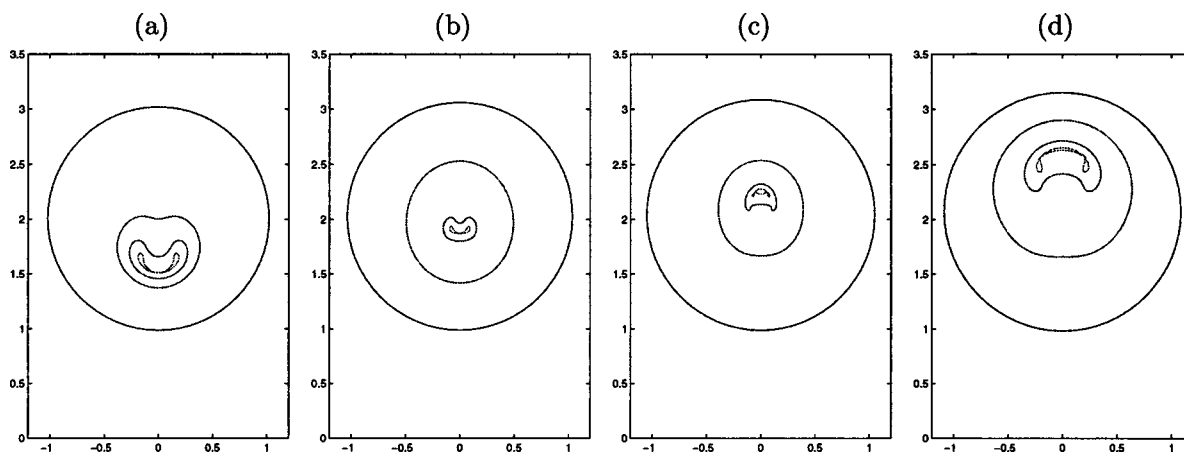


FIG. 9. (Color online) Bubble profiles during collapse phase for $\gamma=2$, $\alpha=0$, $R_0=0.1$, and $\beta=0.1$. From leftmost to rightmost: $\delta=0, 0.04, 0.06$, and 0.1 . In the subfigures, from outermost to innermost, the nondimensional times are (a) 0.932, 1.819, 1.846, 1.856; (b) 0.976, 1.871, 1.954, 1.957; (c) 1.015, 1.976, 2.022, 2.024; (d) 1.107, 2.046, 2.180, 2.202.

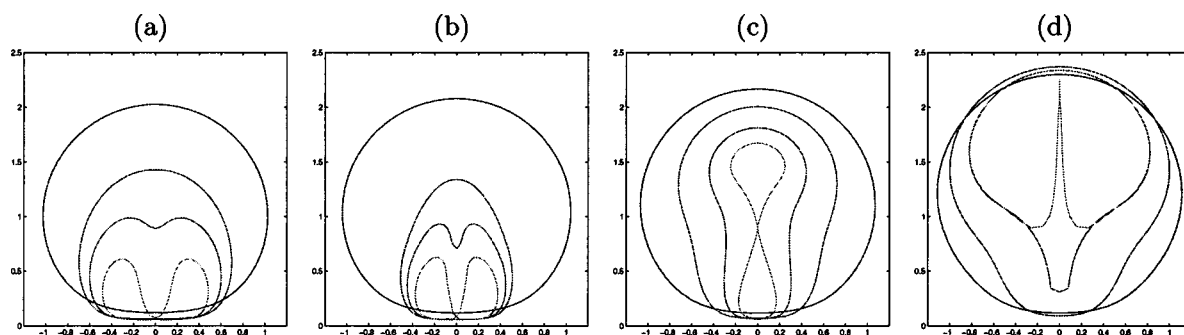


FIG. 10. (Color online) Bubble profiles during collapse phase for $\gamma=1$, $\alpha=0$, $R_0=0.1$, and $\beta=0$. From leftmost to rightmost: $\delta=0, 0.05, 0.12$, and 0.2 . In the subfigures, from outermost to innermost, the nondimensional times are (a) 1.092, 1.926, 2.042, 2.145; (b) 1.153, 2.164, 2.214, 2.262; (c) 1.240, 2.129, 2.365, 2.447; (d) 1.380, 2.027, 2.448, 2.453.

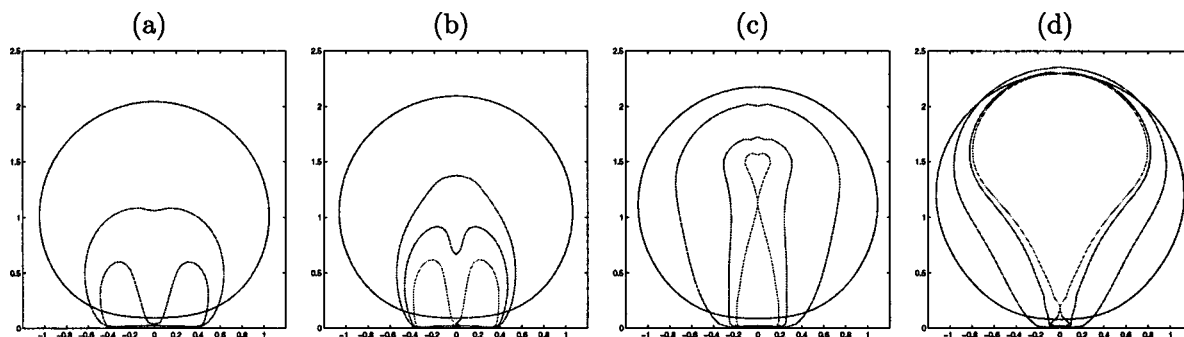


FIG. 11. (Color online) Bubble profiles during collapse phase for $\gamma=1$, $\alpha=0$, $R_0=0.1$, and $\beta=0.05$. From leftmost to rightmost: $\delta=0, 0.05, 0.12$, and 0.2 . In the subfigures, from outermost to innermost, the nondimensional times are (a) 1.065, 1.959, 2.084; (b) 1.120, 2.078, 2.138, 2.189; (c) 1.205, 2.024, 2.314, 2.358; (d) 1.336, 2.051, 2.325, 2.365.

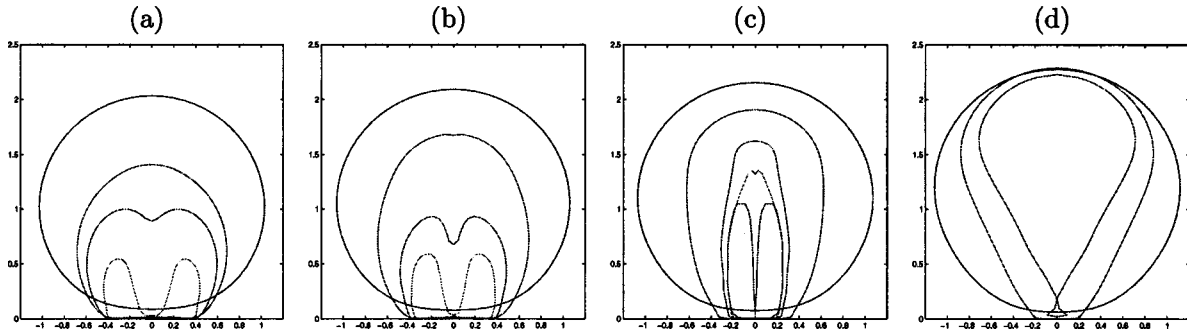


FIG. 12. (Color online) Bubble profiles during collapse phase for $\gamma=1$, $\alpha=0$, $R_0=0.1$, and $\beta=0.1$. From leftmost to rightmost: $\delta=0, 0.05, 0.12$, and 0.2 . In the subfigures, from outermost to innermost, the nondimensional times are (a) 0.987, 1.773, 1.866, 1.980; (b) 1.061, 1.850, 2.034, 2.094; (c) 1.111, 2.022, 2.164, 2.181, 2.188; (d) 1.250, 2.215, 2.261.

stability induced by the high fluid velocity and suffers the dissipative type instability induced by the surface tension terms so that the maximal allowed time step Δt is much smaller than the grid spacing. Therefore, even if the system of ordinary differential equations is solved by a lower order scheme the accuracy in time integration can also be ensured. In this paper the system of ordinary differential equations is solved by the Eulerian method. At any time t the time step Δt is dynamically taken to be

$$\Delta t = \frac{\Delta t_0}{1 + \frac{1}{2}u_{\max}^2 + \alpha(V_0/V)^\kappa + \beta c_{v \max}}$$

where u_{\max} and $c_{v \max}$ are, respectively, the maximal bubble velocity and bubble curvature at time t and Δt_0 is the initial time step. In calculations, the larger the value of β is, the smaller the value of Δt_0 should be taken. For example, when $\gamma=1.5$ and $\alpha=0$, in this paper, for $\beta=0, 0.05$ and 0.1 , Δt_0 is taken as 0.01, 0.005, and 0.0025, respectively.

In order to avoid the nonlinearly numerical instability induced by the accumulation of markers on the bubble surfaces it is necessary to use grid reconstruction techniques. The grid reconstruction technique based on the usual interpolation of high-order polynomials or splines will cause unwanted nu-

merical oscillations. To suppress the numerical oscillations it is necessary to employ some artificial smoothing techniques without any physical meaning. In this paper the used grid reconstruction method is based on the essentially nonoscillatory (ENO) interpolation of third order polynomials [25], which can remove the numerical oscillations without employment of any artificial smoothing technique.

III. NUMERICAL RESULTS

The numerical experiments contain two parts. The first part is for pure vapor cavities ($\alpha=0$) and in this part all of the cavities have the same initial dimensionless radius $R_0=0.1$, as was done in Ref. [19]. The second part is for cavities containing some noncondensable contents ($\alpha=100$) and in this case all of the cavities have the same initial dimensionless radius $R_0=0.1651$, as was done in Ref. [17]. For $\gamma=1.5$, $\alpha=0$, $\beta=0$, $\delta=0$, and $R_0=0.1$, Fig. 1 gives the computed bubble profile, velocity field, and pressure contours just before jet impact. The results are almost exactly the same as those shown in Fig. 7(a) and Fig. 9(a) in Ref. [19] for the same case. So it is believable that there are no mistakes in the mathematical derivations and programming of this paper.

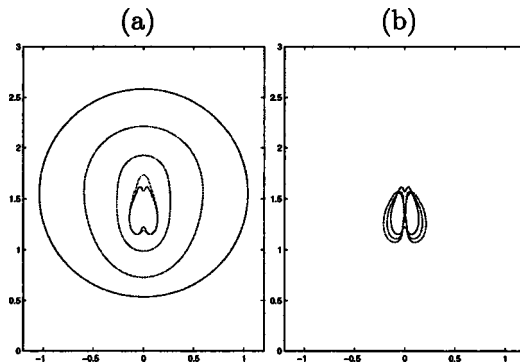


FIG. 13. (Color online) Bubble profiles during the collapse and rebound phases for $\gamma=1.5$, $\alpha=100$, $\delta=0.053$, $R_0=0.1651$, and $\beta=0$. (a) Collapse phase. From outermost to innermost, $t=1.141, 2.144, 2.311, 2.351, 2.356$. (b) Rebound phase. From innermost to outermost, $t=2.356, 2.368, 2.376$.

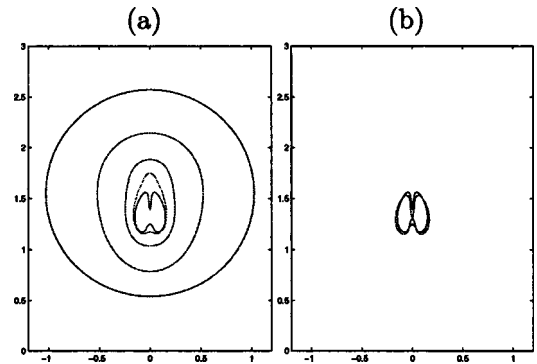


FIG. 14. (Color online) Bubble profiles during the collapse and rebound phases for $\gamma=1.5$, $\alpha=100$, $\delta=0.053$, $R_0=0.1651$, and $\beta=0.01$. (a) Collapse phase. From outermost to innermost, $t=1.152, 2.143, 2.268, 2.294, 2.305$. (b) Rebound phase. From innermost to outermost, $t=2.305, 2.314$.

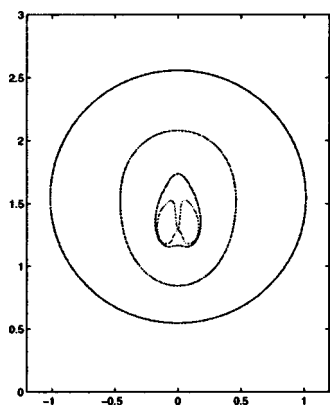


FIG. 15. (Color online) Bubble profiles during the collapse phase for $\gamma=1.5$, $\alpha=100$, $\delta=0.053$, $R_0=0.1651$, and $\beta=0.02$. From outermost to innermost, $t=1.125, 2.130, 2.240, 2.258$.

Before we discuss the numerical results, let us first analyze the mechanism of the jet formation near a transient bubble in a liquid. When an initially spherical bubble in an infinite liquid is only acted on by the buoyancy force, during its motion the flow around the bubble is from its forehead to its rear where the flow is blocked and the pressure is increased, which causes a liquid jet to form there and penetrate the bubble. Suppose an initially spherical cavity generated by a spark or laser experimentally in a stationary liquid is only acted on by the pressure difference $\Delta p = p_\infty - p_c$ and is growing and collapsing near a rigid wall. The pressure difference has the tendency to reduce the volume of the cavity. Therefore during the growth phase the pressure difference will have the effect of resisting the deformation of the cavity and thus to stabilize the physical process and help the cavity keep a spherical shape, whereas during the collapse phase, the pressure difference will have the effect of accelerating the deformation of the cavity and thus to destabilize the physical process so that any nonspherical disturbance to the cavity will make the cavity deviate greatly from a spherical shape. Because of the resistance of the wall to the change of the width of flow channel between the cavity and the wall due to the infinite inertia of the solid wall, during the growth phase the centroid of the cavity will move away from the wall,

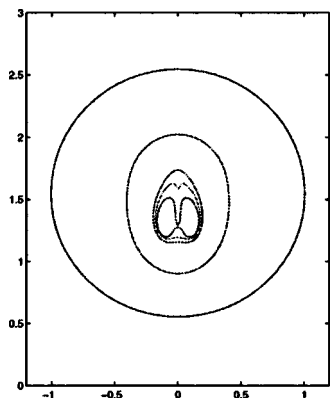


FIG. 16. (Color online) Bubble profiles during the collapse phase for $\gamma=1.5$, $\alpha=100$, $\delta=0.053$, $R_0=0.1651$, and $\beta=0.03$. From outermost to innermost, $t=1.102, 2.109, 2.188, 2.195, 2.207$.

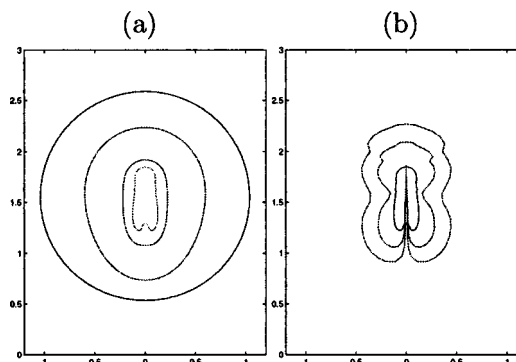


FIG. 17. (Color online) Bubble profiles during the collapse and rebound phases for $\gamma=1.5$, $\alpha=100$, $\delta=0.056$, $R_0=0.1651$, and $\beta=0$. (a) Collapse phase. From outermost to innermost, $t=1.171, 2.149, 2.334, 2.361$. (b) Rebound phase. From innermost to outermost, $t=2.361, 2.417, 2.500$.

whereas during the collapse phase its centroid will move to the wall so that the flow around the cavity will be from its near wall side to the opposite side, causing the flow to be blocked near its far side from the wall and increase of the liquid pressure there, which will cause a wall-directed jet to form and develop there. The force induced by the presence of a solid wall that makes the centroid of the cavity move to the wall is called the Bjerknes force, which decreases when the distance between the cavity and the wall increases. When an initially spherical cavity growing and collapsing near a rigid wall is acted on by both the buoyancy force and the pressure difference, during the collapse phase the direction of the liquid jet will depend on the direction of the resultant force of the two forces at the late stage of the collapse.

Because surface tension has the effect of reducing the area of a bubble and thus reducing its volume and generating an inward pressure on the surface of a convex bubble, which is similar to that of a pressure difference, for an initially spherical cavity growing and collapsing near a rigid wall, during the growth phase surface tension will have the effect of stabilizing the deformation of the cavity and make it closer to a spherical shape, and during the collapse phase surface tension will have the effect of destabilizing the deformation of

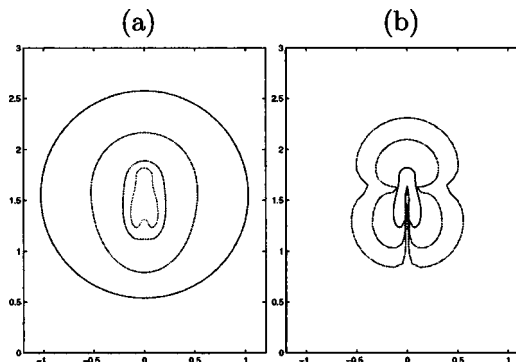


FIG. 18. (Color online) Bubble profiles during the collapse and rebound phases for $\gamma=1.5$, $\alpha=100$, $\delta=0.056$, $R_0=0.1651$, and $\beta=0.01$. (a) Collapse phase. From outermost to innermost, $t=1.151, 2.149, 2.286, 2.311$. (b) Rebound phase. From innermost to outermost, $t=2.311, 2.381, 2.503$.

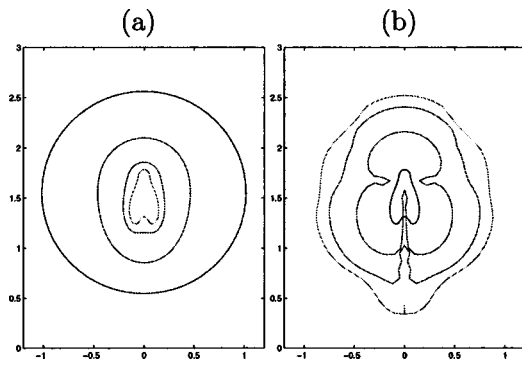


FIG. 19. (Color online) Bubble profiles during the collapse and rebound phases for $\gamma=1.5$, $\alpha=100$, $\delta=0.056$, $R_0=0.1651$, and $\beta=0.02$. (a) Collapse phase. From outermost to innermost, $t=1.124$, 2.137, 2.239, 2.259. (b) Rebound phase. From innermost to outermost, $t=2.259$, 2.385, 2.624, 2.874.

the cavity, accelerating the collapse, and helping its centroid move to the wall, and thus will have the tendency to strengthen the wall effects.

When $\gamma=1.5$, $\alpha=0$, and $R_0=0.1$, for $\beta=0, 0.05$, and 0.1 , Figs. 2–4, respectively, give the computed bubble profiles during the collapse phase for different values of δ . It can be seen that for cases where $\delta < 0$ or $0 \leq \delta \leq 0.05$, when surface tension effect is neglected ($\beta=0$), at the late stage of the collapse the resultant force of the Bjerknes force and the buoyancy force is directed to the wall so that the liquid jet is also directed to the wall and after jet impact a toroidal bubble forms. In these cases the surface tension effect cannot change the direction of the jet but only makes it a little stronger (wider) and makes the bubble elongation along the axisymmetric axis reduced. For cases where $\delta \geq 0.1$, when $\beta=0$, at the late stage of the collapse the buoyancy force is stronger than the Bjerknes force so that the resultant force is directed away from the wall and the jet is also directed away from the wall, and after jet impact a toroidal bubble forms. In these cases, at the late stage of the collapse the buoyancy force is strong enough so that when $\beta=0.05$ and 0.1 , although the surface tension effect strengthens the wall effect it cannot change the direction of the resultant force and therefore can-

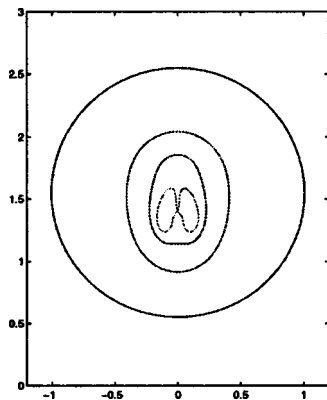


FIG. 20. (Color online) Bubble profiles during the collapse phase for $\gamma=1.5$, $\alpha=100$, $\delta=0.056$, $R_0=0.1651$, and $\beta=0.03$. From outermost to innermost, $t=1.097$, 2.117, 2.186, 2.220.

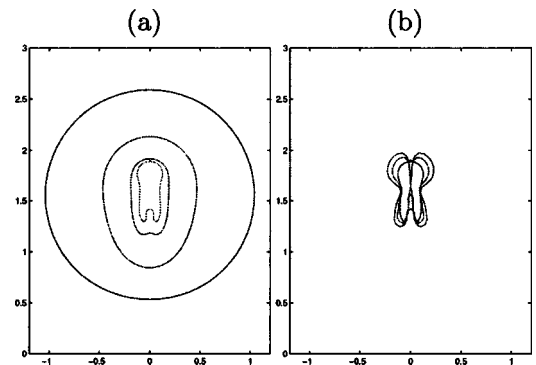


FIG. 21. (Color online) Bubble profiles during the collapse and rebound phases for $\gamma=1.5$, $\alpha=100$, $\delta=0.058$, $R_0=0.1651$, and $\beta=0$. (a) Collapse phase. From outermost to innermost, $t=1.185$, 2.246, 2.350, 2.373. (b) Rebound phase. From innermost to outermost, $t=2.373$, 2.389, 2.397.

not change the direction of the liquid jet. For the case of $\delta=0.1$, after jet impact, a toroidal bubble forms when $\beta=0$, a smaller toroidal bubble and a bubble with crescent-shaped meridian section form when $\beta=0.05$, and a tiny toroidal bubble and a bubble with mouth-shaped meridian section form when $\beta=0.1$. However, for the case of $\delta=0.063$, the case where at the late stage of the collapse the buoyancy force and the Bjerknes force are nearly equal in magnitude but are in opposite directions, i.e., the Kelvin impulse acting on the bubble is near zero, the surface tension has significant effects on bubble shapes. In this case, just before jet impact, when $\beta=0$ there are two liquid jets; one is above the upper surface and is directed to the wall, and the other is below the lower surface and is in a direction away from the wall and is much wider and longer than the upper one; when $\beta=0.05$ the lower jet is wider but much shorter and weaker than the upper one; and when $\beta=0.1$ the upper jet is the only one to appear. In the case of $\delta=0.063$, Figs. 5 and 6 give the computed velocity fields and pressure contours for $\beta=0$ and $t=2.259$, and for $\beta=0.1$ and $t=2.041$, respectively. It can be seen that at about the time of jet inception, when $\beta=0$ there are two pressure maxima at the symmetric axis; one is below

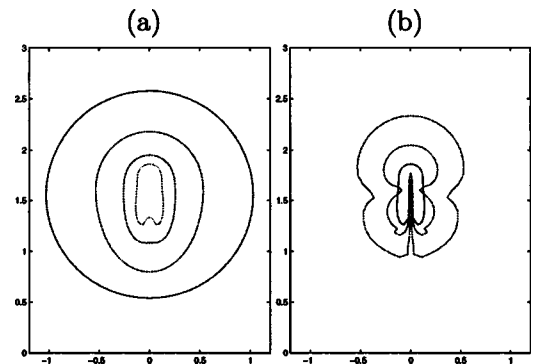


FIG. 22. (Color online) Bubble profiles during the collapse and rebound phases for $\gamma=1.5$, $\alpha=100$, $\delta=0.058$, $R_0=0.1651$, and $\beta=0.01$. (a) Collapse phase. From outermost to innermost, $t=1.152$, 2.152, 2.280, 2.312. (b) Rebound phase. From innermost to outermost, $t=2.312$, 2.359, 2.484.

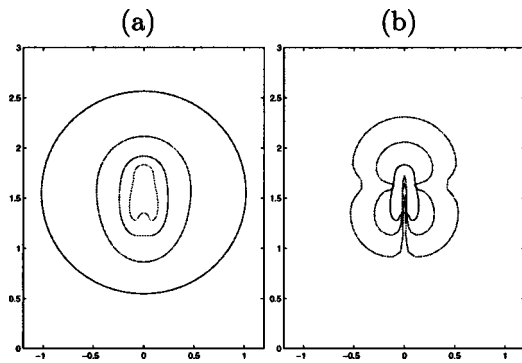


FIG. 23. (Color online) Bubble profiles during the collapse and rebound phases for $\gamma=1.5$, $\alpha=100$, $\delta=0.058$, $R_0=0.1651$, and $\beta=0$. (a) Collapse phase. From outermost to innermost, $t=1.119$, 2.142, 2.235, 2.264. (b) Rebound phase. From innermost to outermost, $t=2.264$, 2.320, 2.449.

the bubble and the other is above the bubble. The pressure gradient near the lower pressure maximum is much higher than that near the upper pressure maximum, which makes the lower jet much larger than the upper one later. When $\beta=0.1$ there appears only one pressure maximum, the one above the bubble. Therefore, in this case at the later stage of collapse there appears only one liquid jet, the one above the bubble, which is caused by the large pressure gradient near the upper pressure maximum.

For the case of $\gamma=1.5$, $\alpha=0$, and $R_0=0.1$, Table I gives the bubble collapse time t_c defined as the difference between the jet impact time and the time when the cavity begins to collapse for different values of δ and β . It can be seen that for same value of δ , t_c decreases when β increases because the surface tension effect accelerates the collapse of the cavity.

When $\gamma=2$, $\alpha=0$, and $R_0=0.1$, for $\beta=0$, 0.05 and 0.1, Figs. 7–9, respectively, give the computed bubble profiles during the collapse phase for different values of δ . It can be seen that the jet is directed to the wall when $\delta \leq 0.04$ and is in the opposite direction when $\delta \geq 0.06$. When the stand-off parameter γ increases the cavity volume at jet impact time decreases. When $\delta \leq 0.04$ or when $\delta \geq 0.1$ the surface tension

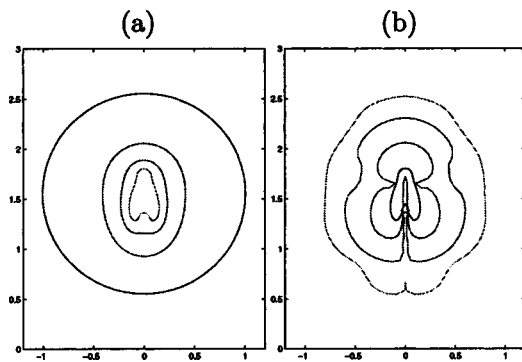


FIG. 24. (Color online) Bubble profiles during the collapse and rebound phases for $\gamma=1.5$, $\alpha=100$, $\delta=0.058$, $R_0=0.1651$, and $\beta=0.01$. (a) Collapse phase. From outermost to innermost, $t=1.109$, 2.122, 2.190, 2.216. (b) Rebound phase. From innermost to outermost, $t=2.216$, 2.281, 2.431, 2.728.

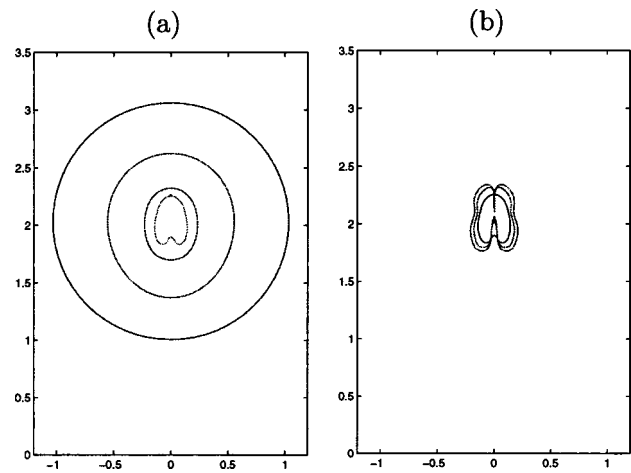


FIG. 25. (Color online) Bubble profiles during collapse and rebound phases for $\gamma=2$, $\alpha=100$, $\delta=0.035$, $R_0=0.1651$, and $\beta=0$. (a) Collapse phase. From outermost to innermost, $t=1.121$, 2.115, 2.252, 2.277. (b) Rebound phase. From innermost to outermost, $t=2.277$, 2.292, 2.300.

has no appreciable effects on bubble shapes except also that the bubble elongation is reduced and the jet becomes shorter and wider so that the volume of the toroidal bubble at jet impact time becomes smaller. For $\delta=0.06$, at jet impact time a toroidal bubble and a bubble with a crescent-shaped meridian section form when $\beta=0$ and a tiny toroidal bubble and a bubble with a mouth-shaped meridian section form when $\beta=0.05$ and $\beta=0.1$.

When $\gamma=1$, $\alpha=0$, and $R_0=0.1$, for $\beta=0$, 0.05, and 0.1 Figs. 10–12, respectively, give the computed bubble profiles during the collapse phase for different values of δ . It can be seen that when γ decreases the cavity volume at jet impact time increases. When $\delta \leq 0.05$ the jet is directed to the wall and the surface tension has no appreciable effects on bubble shapes, but when $\delta=0.12$ or $\delta=0.2$ the surface tension has substantial effects on bubble collapse. For the case of $\delta=0.12$, when $\beta=0$ at the later stage of the collapse an annular jet occurs and at the jet impact time the bubble is pinched off at the middle of its flank and split into two smaller bubbles with almost the same volume; when $\beta=0.05$ the pinching off happens at the upper part of its flank and the lower split bubble is larger than the upper one; but when $\beta=0.1$ at the later stage of the collapse a jet directed to the wall occurs and after jet impact a toroidal bubble forms. For the case of $\delta=0.2$, when $\beta=0$ at the later stage of the collapse a light-bulb-shaped bubble occurs (similar results can be seen in Fig. 5 in Ref. [16]) and then a jet directed away from the wall develops and finally a toroidal bubble forms; but when $\beta=0.05$ and $\beta=0.1$ at the later stage of the collapse an annular jet occurs near the bottom of the bubble and at the jet impact time the bubble is pinched off at the very low part of its flank and split into two bubbles. The upper split bubble is of a light bulb shape and is very much larger than the lower one.

From the preceding results, it can be seen that for a pure vapor cavity, when surface tension effect is neglected, there is a critical value $\eta_c \approx 0.1$ for the product $\eta = \gamma\delta$ such that when $\eta < \eta_c$, at the late stage of the collapse the resultant

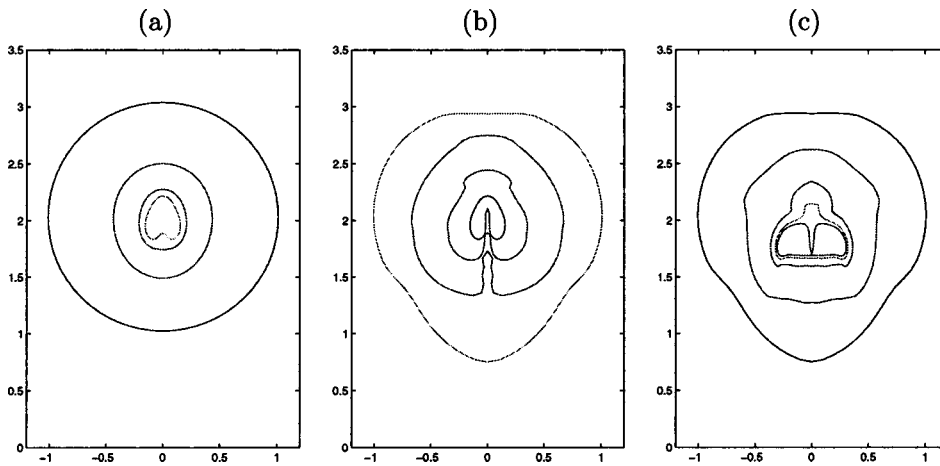


FIG. 26. (Color online) Bubble profiles during collapse, rebound, and recollapse phases for $\gamma=2$, $\alpha=100$, $\delta=0.035$, $R_0=0.1651$, and $\beta=0.02$. (a) Collapse phase. From outermost to innermost, $t=1.081$, 2.085 , 2.162 , 2.181 . (b) Rebound phase. From innermost to outermost, $t=2.181$, 2.237 , 2.431 , 3.260 . (c) Recollapse phase. From outermost to innermost, $t=3.260$, 4.169 , 4.325 , 4.347 , 4.354 .

force of the Bjerknes force and the buoyancy force is directed to the wall and the liquid jet is also directed to the wall, when $\eta > \eta_c$, at the late stage of the collapse the resultant force is directed away from the wall and the liquid jet is also directed away from the wall, and when $\eta \approx \eta_c$, at the late stage of the collapse the resultant force is near zero and an annular liquid jet could occur at the flank of the bubble. In the last case surface tension can have a significant effect on the collapse behavior of the cavity.

Next we discuss the numerical results for a cavity containing some noncondensable contents. When $\gamma=1.5$, $\alpha=100$, $\delta=0.053$, and $R_0=0.1651$, for $\beta=0$, 0.01 , 0.02 , and 0.03 , Figs. 13–16, respectively, give the computed bubble profiles during collapse and rebound phases. It can be seen that when $\beta=0$ at the very late stage of collapse two liquid jets occur; one is below the bubble and the other is above the bubble. After the jets develop a little the bubble stops collapsing and begins to rebound. During the rebound phase the two jets go continuously until they impact each other and a toroidal bubble forms. Before the jets impact the bubble rebound only lasts a very short time and is in a small amount. When $\beta=0.01$ during the collapse phase the two jets go longer and the bubble only rebounds very little before the jets impact. When $\beta=0.02$ and 0.03 the two jets develop continuously during the collapse phase and there is no bubble rebound to occur before the two jets impact.

When $\gamma=1.5$, $\alpha=100$, $\delta=0.056$, and $R_0=0.1651$, for $\beta=0$, 0.01 , 0.02 , and 0.03 , Figs. 17–20, respectively, give the

computed bubble profiles during collapse and rebound phases. It can be seen that when $\beta=0$ at the very late stage of the collapse a liquid jet occurs below the bubble. Also after the jet develops a little, the bubble stops collapsing and starts to rebound. During the rebound phase the jet goes very fast, but no jet impact occurs because the computation fails, since the top part of the jet is too thin to be numerically simulated by a boundary integral method. During the rebound phase some waves appear on the flank of the bubble (the wave phenomenon on a bubble surface during the rebound phase can also be seen in the experiments in Ref. [12]). The rebound lasts a longer time and is in a larger amount than in the case of Fig. 13. When $\beta=0.01$ during the rebound phase at first the thin jet goes very fast but when it reaches its farthest it stops developing and begins to withdraw. At an early time of the rebound a neck forms at the upper part of the bubble flank and then the neck becomes thicker and thicker. At a later time of the rebound a neck occurs on the upper part of the jet. The neck develops and finally the jet is pinched off and the computation fails. When $\beta=0.02$ during the later stage of the rebound the jet withdraws step by step and finally disappears. The neck that occurs on the flank of the bubble at the early time of the rebound becomes thicker and thicker and then disappears; instead, some waves occur on the bubble surface. The rebound lasts a much longer time and in a much larger amount. At a very late time of the rebound a cut appears at the bottom of the bubble and the numerical simulation fails. When $\beta=0.03$ during the collapse

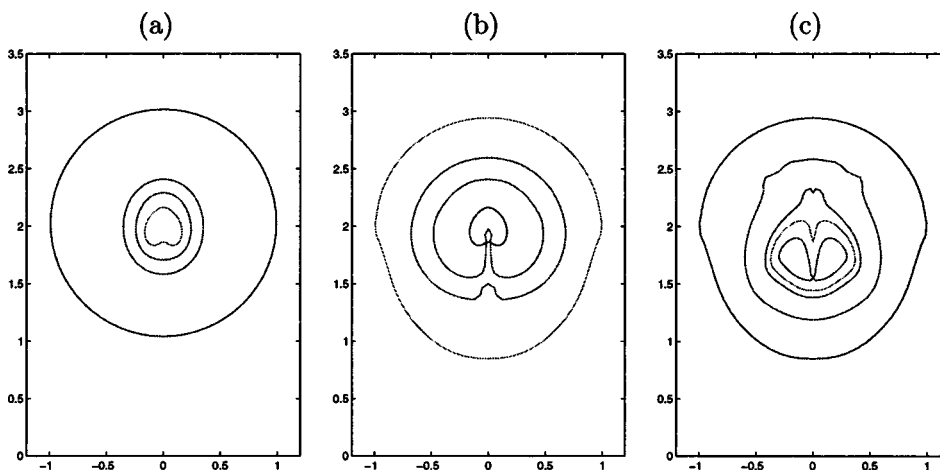


FIG. 27. (Color online) Bubble profiles during collapse, rebound, and recollapse phases for $\gamma=2$, $\alpha=100$, $\delta=0.035$, $R_0=0.1651$, and $\beta=0.04$. (a) Collapse phase. From outermost to innermost, $t=1.052$, 2.029 , 2.062 , 2.088 . (b) Rebound phase. From innermost to outermost, $t=2.088$, 2.190 , 2.323 , 3.208 . (c) Recollapse phase. From outermost to innermost, $t=3.208$, 3.997 , 4.128 , 4.151 , 4.178 .

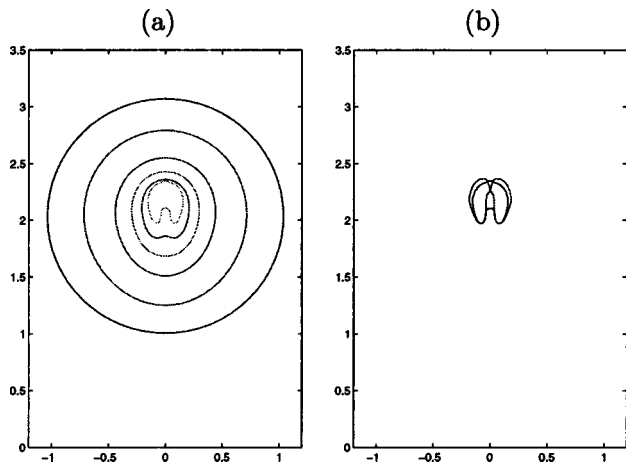


FIG. 28. (Color online) Bubble profiles during collapse and rebound phases for $\gamma=2$, $\alpha=100$, $\delta=0.04$, $R_0=0.1651$, and $\beta=0$. (a) Collapse phase. From outermost to innermost, $t=1.741, 2.002, 2.201, 2.256, 2.280, 2.300$. (b) Rebound phase. From innermost to outermost, $t=2.300, 2.310$.

phase there are two liquid jets, one above the bubble and the other below the bubble; they develop continuously and finally impact each other and a toroidal bubble forms. In this case there is no bubble rebound to occur before the jets impact.

When $\gamma=1.5$, $\alpha=100$, $\delta=0.058$, and $R_0=0.1651$, for $\beta=0, 0.01, 0.02$ and 0.03 , Figs. 21–24, respectively, give the computed bubble profiles during the collapse and rebound phases. It can be seen that when $\beta=0$ at the very late stage of the collapse a liquid jet occurs below the bubble. During the rebound phase another liquid jet appears above the bubble and the two jets develop continuously until they impact each other and a toroidal bubble forms. Before the jets impact the rebound only lasts a very short time and is in a small amount. When $\beta=0.01, 0.02$, and 0.03 , during the rebound phase there is no jet to appear above the bubble and only a very thin jet below the bubble develops. At an early stage of the rebound a neck forms on the flank of the bubble and then becomes thicker and thicker. In the case of $\beta=0.03$ the neck on the bubble finally disappears. When β increases the rebound time and the amount both increase. During the collapse phase the thin jet develops continuously when β

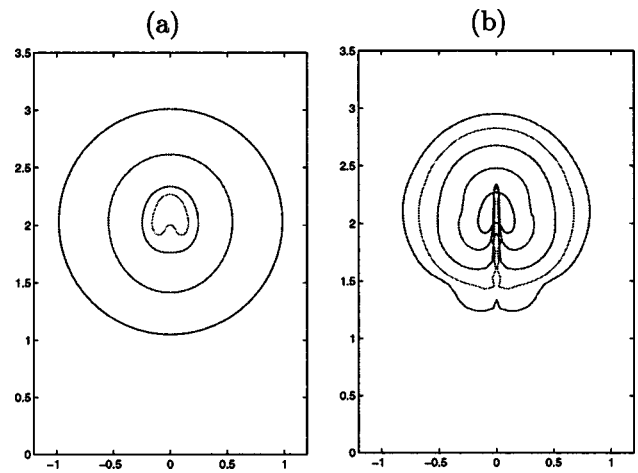


FIG. 29. (Color online) Bubble profiles during collapse and rebound phases for $\gamma=2$, $\alpha=100$, $\delta=0.04$, $R_0=0.1651$, and $\beta=0.05$. (a) Collapse phase. From outermost to innermost, $t=1.007, 1.907, 2.035, 2.063$. (b) Rebound phase. From innermost to outermost, $t=2.063, 2.113, 2.202, 2.322, 2.485$.

$=0.01$, but the jet develops at first and then stops developing and begins to withdraw when $\beta=0.02$ and 0.03 . When $\beta=0.01, 0.02$, and 0.03 at a later time of the rebound a neck occurs at the upper part of the jet. When $\beta=0.01$ and 0.02 the neck on the flank of the jet develops and finally the jet is pinched off and the computation fails. When $\beta=0.03$ at a very late time of the rebound a cut forms at the bottom of the bubble and the computation fails. During the collapse phase for $\beta=0$, or during the rebound phase for $\beta=0.01$ and 0.02 , the bubble shapes are similar to those given in Fig. 5 in Ref. [17].

When $\gamma=2$, $\alpha=100$, $\delta=0.035$, and $R_0=0.1651$, for $\beta=0, 0.02$, and 0.04 , Figs. 25–27, respectively, give the computed bubble profiles during collapse, rebound, and recollapse phases. It can be seen that when $\beta=0$ at the very late stage of the collapse a liquid jet below the bubble occurs. During the rebound phase another very thin liquid jet appears above the bubble and the two jets develop continuously. The computation fails before the two jets impact because at a later time the upper jet is too thin to simulate by a boundary integral method. The rebound only lasts a short time and is in a small amount. When $\beta=0.02$ and 0.04 during the rebound phase no

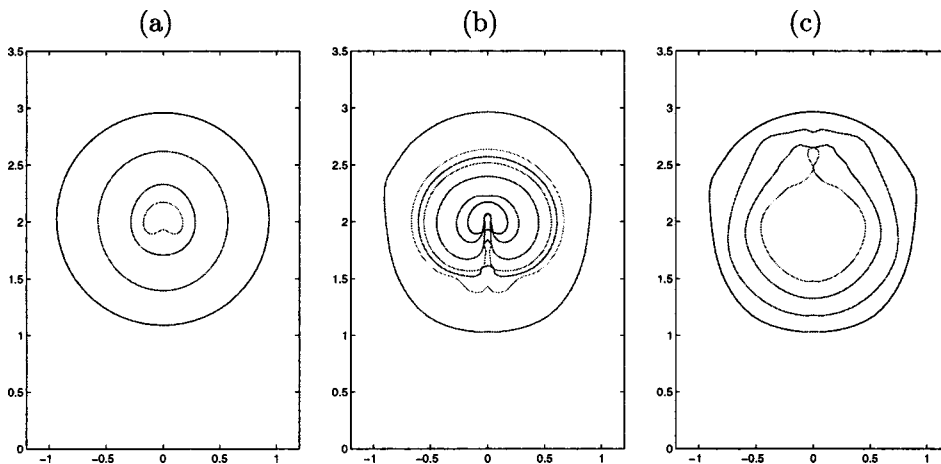


FIG. 30. (Color online) Bubble profiles during collapse, rebound, and recollapse phases for $\gamma=2$, $\alpha=100$, $\delta=0.04$, $R_0=0.1651$, and $\beta=0.1$. (a) Collapse phase. From outermost to innermost, $t=0.918, 1.684, 1.823, 1.859$. (b) Rebound phase. From innermost to outermost, $t=1.859, 1.883, 1.940, 2.000, 2.035, 2.085, 2.785$. (c) Recollapse phase. From outermost to innermost, $t=2.785, 3.359, 3.548, 3.638$.

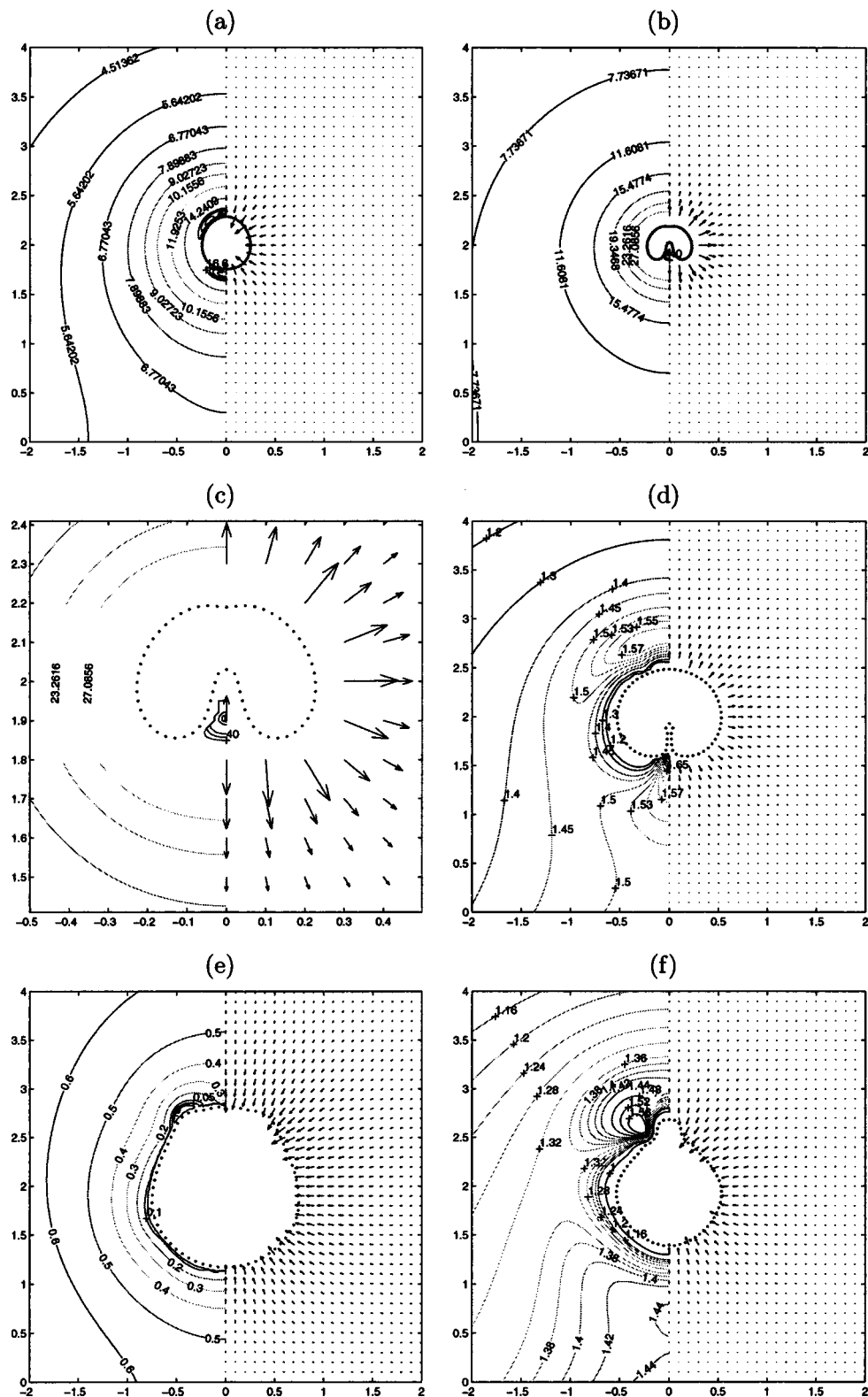


FIG. 31. (Color online) Velocity fields and pressure contours during collapse, rebound, and recollapse phases for $\gamma=2$, $\alpha=100$, $\beta=0.1$, $\delta=0.04$, and $R_0=0.1651$. In the subfigures, the nondimensional times are (a) $t=1.833$, (b) $t=1.873$, (c) $t=1.873$, (d) $t=1.982$, (e) $t=3.359$, and (f) $t=3.594$.

jet appears above the bubble and the jet below the bubble goes quickly at first; when it reaches its maximal length it begins to withdraw step by step and finally the jet disappears completely. The rebound lasts a quite long time and is in a

large amount. When the bubble reaches its maximal volume it begins to collapse again. At the later stage of the recollapse a jet above the bubble occurs and develops until it impacts the lower surface of the bubble and a toroidal bubble forms.

During the recollapse phase the jet appears at a much later time and develops much faster in the case of $\beta=0.02$ than in the case of $\beta=0.04$.

When $\gamma=2$, $\alpha=100$, $\delta=0.04$, and $R_0=0.1651$, for $\beta=0$, 0.05 and 0.1, Figs. 28–30, respectively, give the computed bubble profiles during the collapse, rebound, and recollapse phases. It can be seen that when $\beta=0$ at the very late stage of the collapse a liquid jet below the bubble occurs. During the rebound phase another liquid jet above the bubble appears and the two jets develop continuously until they impact each other and a toroidal bubble forms. The rebound only lasts a very short time and is in a very small amount before the jets impact. When $\beta=0.05$ and 0.1, during the rebound phase no jet appears above the bubble and the jet below the bubble goes quickly at first, and when it reaches its maximal length it stops going and begins to withdraw. The rebound lasts a much longer time and is in a much larger amount. When $\beta=0.05$ during the withdrawal time of the jet some necks appear and develop on the flank of the jet and finally the jet is pinched off and the computation fails. In the case of $\beta=0.1$, when the rebound reaches its farthest the bubble begins to collapse again. At the very late stage of the recollapse an annular liquid jet forms and develops near the upper part of the bubble and finally the bubble is pinched off on its flank and splits into two bubble (the upper one is much smaller than the lower one).

For $\gamma=2$, $\alpha=100$, $\beta=0.1$, $\delta=0.04$, and $R_0=0.1651$, Fig. 31 gives the computed velocity fields and pressure contours at different times. It can be seen from Fig. 31(a) that at the very late time of the collapse ($t=1.833$) there appears a pressure maximum below the bubble and at the symmetric axis. The large pressure gradient near the pressure maximum will cause the liquid jet to form and develop below the bubble. At the beginning of the rebound [Fig. 31(b), $t=1.873$] there is a pressure maximum at the symmetric axis and the interior of the liquid jet. Figure 31(c) is the local amplified diagram near the pressure maximum. Because the liquid mass in the jet pushed by the large pressure gradient near the pressure maximum is very small, the liquid jet is very thin and develops very fast, as observed in Ref. [17]. Just before the jet reaches its maximal length [Fig. 31(d), $t=1.982$] there appear two pressure maxima at the symmetric axis; one is below the bubble, and the other is over the bubble. The two pressure maxima are at a distance from the bubble and the pressure gradient near the two pressure maxima is very small. The actions of the pressure gradient induced by the lower pressure maximum are very weak, so that when the bubble expands the outward liquid flow will cause the thin jet to withdraw from the bubble step by step. At the beginning of the recollapse [Fig. 31(e), $t=3.359$] the liquid flow outside the bubble is in the inward direction and the pressure gradient is in the outward direction, which makes the bubble contract. At the later time of the recollapse [Fig. 31(f), $t=3.594$] there appears a pressure maximum near the upper part of the bubble flank. The large pressure gradient between the bubble and the pressure maximum later causes an annular jet to form.

It can be seen from the preceding results that for a cavity containing some noncondensable content with the parameter $\alpha=100$, when the surface tension effect is neglected, there is

a critical value $\eta_c \approx 0.08$ for the product $\eta = \gamma\delta$ such that when $\eta \approx \eta_c$, at the late stage of the collapse the resultant force of the Bjerknes force and the buoyancy force will be near zero and in this case the surface tension will have substantial effects on the behavior of the cavity.

IV. CONCLUSIONS AND DISCUSSION

By the boundary integral method a numerical investigation is performed for surface tension effects on the behavior of a pure vapor cavity and a cavity containing some noncondensable content, which is growing, collapsing, and rebounding axisymmetrically near a rigid wall for different values of dimensionless stand-off parameter γ , buoyancy parameter δ , and surface tension parameter β . The good agreement between the computed flow field and that given in other work for the same case shows the correctness of the mathematical derivation and the programming of this paper. It is found that at the late stage of the collapse, when the resultant action of the Bjerknes force and the buoyancy force is not small, i.e., when the Kelvin impulse acting on the cavity is not near zero, surface tension has no significant effects on bubble behavior (for example, it cannot change the direction of the liquid jet) except that the collapse time is shortened and the jet becomes wider. Just before the cavity begins to collapse, when the resultant action of the two forces is small enough, i.e., when the Kelvin impulse is near zero, however, surface tension can have significant and in some cases substantial effects on bubble behavior, such as changing the direction of the liquid jet, producing a new liquid jet, in some cases preventing the bubble from rebound before jet impact, and in some other cases causing the bubble to rebound and even recollapse before jet impact. The mechanism of surface tension effects on the collapsing behavior of a cavity has been analyzed. The mechanism of surface tension effects on the rebounding and recollapsing behavior is too complicated for us to analyze, but the analysis of the computed velocity fields and pressure contours of the liquid flow outside the bubble at different stages of the bubble evolution provides a proper illustration for the mechanisms of some phenomena such as the formation of liquid jets, the fast growing and then withdrawing of a very thin liquid jet during the rebound phase, and the recollapse of the bubble.

All of the numerical simulations will fail when the bubble topology changes. In order to make the numerical simulation go further the boundary integral method has to be improved to allow any change of the bubble topology, which is a topic for further research.

In some cavitation problems, such as the laser- or ultrasound-surgery-linked cavitation problems where the Reynolds number of the flow induced by the transient cavity is not very high, the effect of liquid viscosity could be important. Although the viscosity effect on cavity behavior can be studied numerically by the combined boundary integral and boundary layer approximation method [26], the applicability of this method is greatly reduced by its intrinsic defect

that it is accurate only for quite high-Reynolds-number cases where the liquid viscosity effect will be quite small. Therefore this problem should be studied more appropriately by the full-flow-field method. Reference [27] studied this problem by a combined finite volume and free-surface-marker method. This problem can also be studied more efficiently by

the VOF, or level set method, which will be the next step in our work.

ACKNOWLEDGMENT

This work was supported by NSFC Project No. 10272032.

-
- [1] Lord Rayleigh, *Philos. Mag.* **34**, 94 (1917).
 [2] T.B. Benjamin and A.T. Ellis, *Philos. Trans. R. Soc. London, Ser. A* **260**, 221 (1966).
 [3] W. Lauterborn and H. Bolle, *J. Fluid Mech.* **72**, 391 (1975).
 [4] G.L. Chahine, *Appl. Sci. Res.* **38**, 187 (1982).
 [5] Y. Tomita and A. Shima, *J. Fluid Mech.* **169**, 535 (1986).
 [6] A. Vogel, W. Lauterborn, and R. Timm, *J. Fluid Mech.* **206**, 299 (1989).
 [7] A. Philipp and W. Lauterborn, *J. Fluid Mech.* **361**, 75 (1998).
 [8] J.R. Blake, Y. Tomita, and R.P. Tong, *Appl. Sci. Res.* **58**, 77 (1998).
 [9] R.P. Tong, W.P. Schiffers, S.J. Shaw, J.R. Blake, and D.C. Emmony, *J. Fluid Mech.* **380**, 339 (1999).
 [10] S.J. Shaw, W.P. Schiffers, and D.C. Emmony, *J. Acoust. Soc. Am.* **110**, 1822 (2001).
 [11] E.A. Brujan, G.S. Keen, A. Vogel, and J.R. Blake, *Phys. Fluids* **14**, 85 (2002).
 [12] O. Lindau and W. Lauterborn, *J. Fluid Mech.* **479**, 327 (2003).
 [13] M.S. Plesset and R.B. Chapman, *J. Fluid Mech.* **47**, 283 (1971).
 [14] M. Sussman, *J. Comput. Phys.* **187**, 110 (2003).
 [15] G.K. Batchelor, *An Introduction to Fluid Dynamics* (Cambridge University Press, Cambridge, U.K., 1967).
 [16] J.R. Blake, B.B. Taib, and G. Doherty, *J. Fluid Mech.* **170**, 479 (1986).
 [17] J.P. Best and A. Kucera, *J. Fluid Mech.* **245**, 137 (1992).
 [18] J.P. Best, *J. Fluid Mech.* **251**, 79 (1993).
 [19] S. Zhang, J.H. Duncan, and G.L. Chahine, *J. Fluid Mech.* **257**, 147 (1993).
 [20] G.L. Chahine and T.O. Perdue, in *Drops and Bubbles*, edited by T.G. Wang, AIP Conf. Proc. No. 197 (AIP, New York, 1989), pp. 188–199.
 [21] J.R. Blake, M.C. Hooton, P.B. Robinson, and R.P. Tong, *Philos. Trans. R. Soc. London, Ser. A* **355**, 537 (1997).
 [22] Y.L. Zhang, K.S. Yeo, B.C. Khoo, and C. Wang, *J. Comput. Phys.* **166**, 336 (2001).
 [23] J.R. Blake, G.S. Keen, R.P. Tong, and M. Wilson, *Philos. Trans. R. Soc. London, Ser. A* **357**, 251 (1999).
 [24] A.H. Stroud and D. Secrest, *Gaussian Quadrature Formulas* (Prentice-Hall, Englewood Cliffs, NJ, 1966).
 [25] A. Harten, S. Osher, B. Engquist, and S. Chakravathy, *J. Comput. Phys.* **71**, 231 (1987).
 [26] T.S. Lundgren and N.N. Mansour, *J. Fluid Mech.* **224**, 177 (1991).
 [27] S. Popinet and S. Zalesky, *J. Fluid Mech.* **464**, 137 (2002).